Characterization of anthropogenic methane plumes with the Hyperspectral Thermal Emission Spectrometer (HyTES): a retrieval method and error analysis

Le Kuai[1], John Worden[2], King-Fai Li[3], Glynn Hulley[2], Francesca M. Hopkins[2], Charles E. Miller[2], Simon Hook[2], Riley Duren[2], Andrew Aubrey[2]

1. University of Los Angles, Joint Institute for Regional Earth System Science & Engineer
2. Jet Propulsion Laboratory, California Institute of Technology, Pasadena, CA
3. University of Washington, Applied mathematics

Abstract

We introduce a retrieval algorithm to estimate lower tropospheric methane (CH_4) concentrations from surface to 1 km with uncertainty estimates using Hyperspectral Thermal Emission Spectrometer (HyTES) airborne radiance measurements. After resampling, retrievals have a spatial resolution of 6x6 m². Total error from single retrieval is approximately 20%, with the uncertainties determined primarily by noise and spectral interferences from temperature, surface emissivity, and atmospheric water vapor. We demonstrate retrievals for a HyTES flight line over storage tanks near Kern River Oil Field (KROF), Kern County, California and find an extended plume structure in the set of observations with elevated methane concentrations (3.0±0.6 ppm to 6.0±1.2 ppm), well above mean concentrations (1.8±0.4 ppm) observed for this scene. With a 20% estimated precision, plume enhancements with more than 1 ppm are distinguishable from the background noise. HyTES retrievals are consistent with simultaneous airborne and ground-based in situ CH_4 mole fraction measurements within the reported accuracy of approximately 0.2 ppm (or ~8%), due to retrieval interferences related to temperature or H_2O or both.

1   Introduction

Methane (CH_4) is an important greenhouse gas. Although the atmospheric concentration of CH_4 is substantially lower than that of CO_2, the radiative forcing per CH_4 molecule is 20 times greater than that of CO_2 (Ramaswamy, 2001;Solomon and (eds.), 2007). Global concentrations of CH_4 have increased nearly threefold from ~700 ppb since preindustrial Holocene (1000 to 1800 A.D) to ~1850 ppb today (Etheridge et al., 1998;NOAA, 2013) with approximately 60-70% of modern CH_4 emissions from anthropogenic sources (Lelieveld et al., 1998).

Major anthropogenic sources of CH_4 ~~include~~ energy, industrial, agricultural, and waste management sectors (Kirschke et al., 2013). Hence CH_4 levels are often higher than the global mean near areas such as oil fields, coal mines, natural gas systems, and feedlots. Quantifying and reducing uncertainties associated with anthropogenic CH_4 emissions generally depend on the capability to monitor and quantify these emitters or leaky sources, which can have an out-sized impact on anthropogenic CH_4 emissions (e.g., Caulton et al., 2014 and refs therein). These -sized impacts of a few leaky sources is one hypothesis for explaining inconsistencies between top-down and bottom-up estimates of the CH_4 emission inventories for large cities or gas exploration regions (Wunch et al., 2009;Hsu et al., 2010;Wennberg et al., 2012;Peischl et al., 2013;Jeong et al., 2013;Wong et al., 2015;McKain et al., 2015;Kort et al., 2014;Frankenberg et al., 2011).

This study presents a quantitative, robust and reliable retrieval algorithm for estimating concentrations in anthropogenic methane plumes at the 1 – 10 m scale using airborne radiance measurements from the airborne Hyperspectral Thermal Emission Spectrometer (HyTES) (Hook et al., 2013, 2015). HyTES is a pushbroom imaging spectrometer that produces a wide swath Thermal Infrared (TIR) image with high spectral and spatial resolution that incorporates a number of key state-of-the-art technologies developed at JPL. It utilizes 256 spectral channels between 7.5

to 12 micron and 512 spatial pixels cross track with ~2 meter spatial resolution of when observing from low altitude of about ~1000 m (1 km) above ground level (AGL). Previous studies produced maps of methane distributions from airborne hyperspectral TIR sensor radiances using methods such as the Cluster-Tuned Matched Filter Detection (CMF) (Funk, 2001); however, such correlative approaches do not yield quantitative estimates of the methane plume concentrations or the corresponding methane emission rates. Our approach is based on the methane optimal estimation atmospheric retrieval algorithm developed for use the Aura Tropospheric Emission Spectrometer (Worden et al., 2004; Bowman et al., 2006; Worden et al., 2012). This method quantifies the estimation uncertainties and vertical sensitivity of the estimate using a Bayesian approach.

HyTES has collected imagery data during flights over the extent of the Kern River Oil Field (KROF), Kern County, California, the different times during February 2015. This paper focuses on describing a retrieval algorithm to quantify CH_4 concentrations based on these HyTES TIR radiances (section 2 and 3). We show the retrieval results for the flight line measured on February 5, 2015, in which a large scale and well developed methane plume is mapped (section 4). In section 5, the retrieval estimated background and plume values are cross-compared with nearby in-situ measurements from airborne and on-road sensors. The conclusions are summarized in section 6. The analysis of more retrieval results for other flight lines will be discussed in the future papers.

2   Retrieval strategy

We apply the retrieval algorithm originally designed for the remote sensing measurements from Tropospheric Emission Spectrometer (TES) on board of the Earth Observing System's Aura Satellite to HyTES spectra from 7.5 to 9.2 micron band to estimate CH_4 mixing ratios in the boundary layer. The major modification of the TES forward model to simulate measured radiances by the airborne HyTES is to

correct the optical path since the observational instrument is now located about 1 km above the ground instead of above the top of the atmosphere.

2.2 HyTES CH$_4$ spectral windows

We use radiances from 7.5 to 9.2 microns (or 1092.3 to 1329.8 wavenumber), which includes the methane band at approximately 8.5 microns to estimate methane. The spectral resolution of approximately 0.0176 microns or 2.12 wavenumber results in a total of 93 spectral measurements per observations. In Figure 1 the black line shows an example of HyTES measured radiances. There is strong interference in this region from water vapor (H$_2$O) and nitrous oxide (N$_2$O), some interference by ozone (O$_3$), and weak interference from carbon dioxide and few low concentration gases. Thus, we simultaneously retrieve H$_2$O and N$_2$O with CH$_4$ and input the empirical profiles for the other interference gases in the forward model. Atmospheric temperature, surface temperature, and emissivity also affect the observed radiance and are therefore simultaneously retrieved with these trace gases during the inversion iterations.

2.3 Forward model and *a priori* vectors

To simulate radiances observed by the HyTES airborne sensor, the radiative transfer model is driven by a realistic temperature/pressure, surface temperature, atmospheric trace gas concentrations, cloud, and emissivity (Bowman et al., 2006). The forward model is based on the Line-By-Line Radiative Transfer Model (LBLRTM) (Worden et al., 2006) (Alvarado et al., 2012). The *a priori* surface temperature, atmospheric temperature, and water vapor profiles are taken from the National Centers for Environmental Prediction/National Center for Atmospheric Research (NCEP/NCAR) Reanalysis dataset for the appropriate time and location (Kalnay et al., 1996).

Simulated high-resolution forward model radiances are convolved with the HyTES instrument line shape (ILS) function and sampled to the center wavenumber of each HyTES measured frequency. For example, Figure 1 shows a comparison between a HyTES radiance measurement and the forward model radiance based on *a priori* atmospheric profile. Differences between the measurement and model reflect differences in the actual and *a priori* temperature, H_2O, methane, and surface emissivity. Surface temperature and emissivity *a priori* information are derived by atmospherically correcting the HyTES radiance data using an in-scene atmospheric correction (ISAC) approach (Young et al., 2002). The advantage of the ISAC method is that atmospheric correction is accomplished using the hyperspectral data itself without the need for external atmospheric profiles. In addition the issue of spectral band misregistrations is eliminated. The Temperature Emissivity Separation (TES) algorithm (Gillespie et al., 1998) is then applied to the atmospherically corrected radiances to produce a surface temperature and spectral emissivity for the HyTES bands. This approach is currently being used to produce the HyTES Level-2 products available at http://www.jpl.nasa.gov/order.

2.4 Retrieval methodology

The observed radiances (y) by HyTES can be described as the sum of model-calculated radiances ($f(x)$) and the residuals (ε) between two of the radiances.

$$y = f(x) + \varepsilon . \qquad (1)$$

The retrieval algorithm uses an optimal estimation approach (Rodgers, 2000;Bowman et al., 2006). Based on this approach, the estimate can be related to the "true state" (in this case the true distribution of methane, temperature, H_2O, etc.) in the form of the following equation:

$$\hat{x} = x_a + \mathbf{A}(x_a - x) + \mathbf{G}n , \qquad (2)$$

where $\hat{x}$, x_a and x are the retrieved, a priori, and the "true" state vectors respectively. The state vectors for trace gases, such as H_2O, CH_4, and N_2O, are expressed in natural logarithm of volume mixing ratio (VMR). However, atmospheric temperature, surface temperature, and surface emissivity are all retrieved linearly. We simultaneously estimate all of these parameters; therefore the state vector is given by a combination of these parameters, i.e.,:

$$x = \begin{Bmatrix} \ln(q_i^{CH4}) \\ \ln(q_i^{H2O}) \\ \ln(q_i^{N2O}) \\ T_i \\ T_{surface} \\ \varepsilon_j \end{Bmatrix} \qquad (3)$$

Where the symbol "q" refers to concentration in VMR at atmospheric level "i". The "T_i" is a profile of atmospheric temperature and the "ε_j" is the surface emissivity as a function of wavelength "j". For the retrievals shown here we estimate three levels of the atmosphere. The "n" is a vector of measurement noise on the spectral radiances. The signal-to-noise ratio (SNR) for HyTES measurements varies between 100 and 180 as a function of frequency at the window region for CH_4 retrieval. $G = \dfrac{\partial x}{\partial y}$ is the gain matrix, mapping from radiance space into profile space. The averaging kernel, $\mathbf{A}$, describes the sensitivity of the retrieved state to the true state:

$$\mathbf{A} = \frac{\partial \hat{x}}{\partial x} = \mathbf{H}\mathbf{K}^{\mathrm{T}}\mathbf{S}_n^{-1}\mathbf{K} = \mathbf{G}\mathbf{K}, \qquad (4)$$

where $\mathbf{K} = \dfrac{\partial \mathbf{y}}{\partial \mathbf{x}}$, is the sensitivity of the forward model radiances to the state vector.

$\mathbf{H}$ is the Hessian matrix, which also represents the covariance matrix for the *posterior* state:

$$\mathbf{H} = (\mathbf{K}^T \mathbf{S}_n^{-1} \mathbf{K} + \mathbf{S}_a^{-1})^{-1}. \qquad (5)$$

$\mathbf{S}_n$ is a covariance matrix for measurement error, a diagonal matrix representing expected errors resulting from spectral noise that is calculated using the noise equivalent temperature difference (NEDT) for the HYTES sensor. $\mathbf{S}_a$ is a covariance matrix for *a priori* state.

2.5 Error analysis

We can characterize the error budget from a single retrieval with the knowledge of the uncertainties of the *a priori* state and the measurement noise (Kuai et al., 2014). The error in the retrieved state is its difference to the true state:

$$\delta x = \hat{x} - x = (\mathbf{I} - \mathbf{A})(x_a - x) + \mathbf{G}\varepsilon_n, \qquad (6)$$

where '$\mathbf{I}$' is a ~~identical~~ matrix. The three terms on the right-hand side of this equation is composed of smoothing error, measurement error, and systematic error.

The total error covariance matrix after retrieval is

$$\hat{\mathbf{S}} = (\mathbf{I} - \mathbf{A})\mathbf{S}_a(\mathbf{I} - \mathbf{A})^T + \mathbf{G}\mathbf{S}_n\mathbf{G}^T + \mathbf{G}\mathbf{K}_b\mathbf{S}_b(\mathbf{G}\mathbf{K}_b)^T \qquad (7)$$

Since we are most interested in the error for the target gas (CH_4), the submatrix of the total error covariance matrix for CH_4 can be rewritten, by separating ~~a~~

covariance for a cross-state error from the covariance for the smoothing error (e.g., (Worden et al., 2004)), as

$$\hat{\mathbf{S}}_{uu} = (\mathbf{I} - \mathbf{A}_{uu})\mathbf{S}_a^{uu}(\mathbf{I} - \mathbf{A}_{tg})^T + \mathbf{A}_{uv}\mathbf{S}_a^{vv}(\mathbf{A}_{uv})^T + \mathbf{GS}_n\mathbf{G}^T,$$
(8)

where subscript 'u' refers to the state vector for the target gas and 'v' refers to simultaneously retrieved parameters other than CH_4. Therefore, $\mathbf{A}_{uu}$ represents the submatrix of $\mathbf{A}$ that is associated with the state vector for CH_4. The same applies to $\mathbf{S}_a^{uu}$ and $\mathbf{S}_a^{vv}$. $\mathbf{A}_{uv}$ refers to the submatrix of $\mathbf{A}$ that relates the sensitivity of the vector 'u' to the vector of 'v'. With this equation, we can attribute the contribution of each ~~the~~ error term in the total error.

3   Retrieval results and error budget

Figure 1 shows an example of the retrieved radiances (red) fitting with the observed radiances (black) much better than *a priori* radiances (blue). In the bottom plot, the residuals become random and symmetric about zero after retrieval. Figure 2 shows how the retrieved profiles of H_2O, CH_4, N_2O, and atmospheric temperature compared with their *a priori* profiles, as well as for the surface temperature.

We used an *a priori* "covariance" matrix for methane to regularize the methane retrieval. This covariance has diagonal values of 0.32 (squared) and off-diagonal values of the empirical correlations between levels. We find this covariance results in a Degrees-Of-Freedom for Signal (DOFS) of approximately 1 (for the retrieval shown in Figure 3, we obtain 0.7). With this DOFS, we expect to observe variations that are larger than the calculated posterior uncertainties that are partly based on the *a priori* covariance. Note that detection of plumes partly depends on the vertical distribution of the plume. For example, the averaging kernel shown in Figure 3 peaks at approximately 0.6 km above the surface. If plume concentrations are all below HyTES most sensitive level (0.6 km), for example when boundary layer height

is below 0.6 km, the plume will be trapped primarily near the surface (where the averaging kernel is approximately 0.15) then it will be more challenging to detect the enhancement with these retrievals.

We find that the a *posteriori* uncertainty for the observed methane column (or average of the observed CH_4 for the three retrieved atmospheric levels) is approximately 20%, for example 0.4 ppm for a background value of 2 ppm (see Figure. 3). The dominant sources of the total error are the smoothing error, measurement error, atmospheric temperature error, H_2O error, and emissivity error. The contributions of surface temperature, and N_2O error to the total error are quite small.

4   Mapping and ~~quantify~~ a methane plume from HyTES data

We ran the CH_4 retrievals of HyTES observations acquired from one flight line collected over one of many active plumes, west of the KROF, on February 5th, 2015. The majority of detected point sources ~~are originated~~ from storage tanks (detected by cluster matched filter; Hulley, *et al.*, 2015).

An image of 1000 by 512 pixels is originally taken, covering approximately 2 km² area centered about 35° latitude and 119° longitude. The radiance measurements are resampled every 3 by 3 pixels to reduce the measurement noise and reduce computational time. Therefore, the spatial resolution of a single target retrieval is now 6×6 m² after the resampling.

A map of the retrieved CH_4 concentrations in the boundary layer is shown along with an image of CH_4 concentration variability calculated using CMF method (Hulley *et al.*, 2015) in Figure 4. Both of them are the cut-off area over the plume. In the CMF image, the intensity of white pixels corresponds to higher concentrations of methane. Both images consistently show a large-scale and well-developed CH_4

plume with maximum enhancements relative to background right above several storage tanks at the surface. Elevated CH_4 concentrations are observed in the plume in excess of 3±0.6 ppm within box **b** in Figure 4 with a maximum enhancement of 6±1.2 ppm and decreasing towards the downwind side and spread over a larger area (Figure 4 box **c** and **d**). Lower concentrations of about 1.8 ppm are observed for the rest of this scene presenting a background region (such as box a). Some scattered, high-biased concentrations of approximately 2.3 ppm are observed away from the plume or at the upwind side of the point source that are likely artifacts of spectral interference ~~from temperature~~ and H_2O because they co-vary with their retrieved quantities and because they are within the calculated uncertainties. Note that the uncertainties are not necessarily a normal distribution as they also depend on variations in the interfering quantities such as temperature and H_2O. Consequently, methane variations at these levels are very difficult to distinguish from the background variations given the estimated uncertainties of ~20% (or ~0.5 ppm).

We used chi-square less than 1.2 as the quality control, where chi-square is the root mean square of the ratio of spectral residuals to the measurement noise. White pixels are those bad retrievals fail to pass the quality flag. For example, two blocks at upper right side away from the point source are estimated of unusually elevated CH_4 for more than 7 ppm, which are resulting from abnormal large negative thermal contrasts.

Figure 5 (a) show that the distributions for methane concentrations over the hotspot area (box (b), (c) and (d) in Figure 4) are distinguishable from the distributions of background areas (box (a)). The signal of those significant enhancements over the storage tanks is larger than the background uncertainties. The distribution for the plume in the box (b) displays a nice long tail structure. Similar asymmetric distribution is found for box (c) and (d), outflows of the emission followed wind direction. For the background areas, the histogram in box (a) has more of a Gaussian distribution.

5   Comparison of HyTES to airborne and ground-based in situ CH₄

A methane profile was measured in tandem with HyTES flights on Feb. 5 by an instrumented aircraft used by the CARVE (Carbon in Arctic Reservoirs Vulnerability Experiment) project during its winter downtime (Miller and Dinardo, 2012). CARVE uses rapid response cavity ring down spectroscopy (G1401, Picarro Inc.) to measure CH_4 (as well as CO_2 and CO) in flight, and records temperature, pressure, and location. CARVE data were collected by flying toward and away from the plume area within the boundary layer (between 963 to 979 mbar), and then spiraling up in a larger area to get the vertical profile in the free troposphere between 963 mbar and 692 mbar. For the lower boundary layer (i.e., below 979 mbar), surface CH_4 observations were used from vehicle transects that intersected the plume. The vehicle observations were made by an on-board G2401 (Picarro, Inc.) that was calibrated against the G1401 on CARVE.

Within the boundary layer, we divided CARVE and on-road data into in plume and out of plume measurements, giving us two profiles to represent the plume profile and background profile (Figure 6). The two profiles, interpolated from three atmospheric levels (i.e., surface to 979 mbar from on-road, 979 to 963 for airborne in boundary layer, and 963 to 897 for the free troposphere in the HyTES partial column), are then convolved with the HyTES averaging kernel and CH_4 *a priori* constraint which represents the HyTES "instrument" function that accounts for the instrument characteristics and retrieval approach for HyTES methane estimates with the following equation

$$\hat{x} = x_a - \mathbf{A}(x - x_a) \quad (9)$$

Table 1 summarizes the vertical average of CH_4 below 1 km at both background region and plume area by CARVE and HyTES. The quantitative retrievals of HyTES data suggest the background of the whole area is 1.80±0.20 ppm, consistent with the in situ CH_4 measurements convolved with averaging kernel. The bias of 0.22 ppm to

in situ data is consistent with the estimated systematic error of 6~7% due to temperature or H_2O bias or both (see Figure 3). The precision of 0.20 ppm is consistent with the estimated random error of 8% from measurement noise. The average of the plume pixels (>2.2 ppm) in box (**b**) is 2.86 ppm, very close to the value of the plume measured in situ. The errors due to temperature and H_2O is in form of random errors increase the precision to 0.62 ppm.

6   Conclusions

In this study, we estimated CH_4 concentrations in one of many active plumes in the Kern River Oil Field using airborne thermal IR radiance measurements from HyTES flying at approximately 1 km AGL. The DOFS for a retrieval of CH_4 concentration from HyTES measurements is close to 1. The uncertainties are about 20% of the estimated CH_4 concentrations for an integrated column between the surface and aircraft. The primary sources of the uncertainties are found to be measurement noise, atmospheric temperature, surface emissivity, and H_2O. Minor errors are introduced by N_2O and surface temperature.

Enhanced methane concentrations of approximately 3±0.6 to 6±1.2 ppm are observed above some storage tanks. The background values around this region are approximately 1.8±0.2 ppm. This methane source is observed continuously releasing elevated methane during other HyTES flight lines on Feb. 8 and 9, 2015. This background value of 1.8 ± 0.2 ppm is consistent with aircraft measurements of background methane in the region of approximately 2 ppm as the accuracy of the HyTES data is approximately 8% or ~0.16 ppm

A future study will apply this retrieval algorithm to a larger number of point sources and cross compare the HyTES quantitative retrievals with in situ measurements, such as road data or other airborne observations, such as CARVE and the Next

Generation Airborne Visible Infrared Spectrometer (AVIRIS-NG) during a multi-aircraft, multi-platform campaign.

Acknowledgements. We would like to thank all other HyTES team members and the pilots for making the measurements and calibrating the data. This research was carried out at the Jet Propulsion Laboratory, California Institute of Technology, under a contract with the National Aeronautics and Space Administration.

References

Bowman, K. W., Rodgers, C. D., Kulawik, S., Worden, J., Sarkissian, E., Osterman, G., Steck, T., Lou, M., Eldering, A., Shephard, M., Worder, H., Lampel, M., Clough, S., Brown, P., Rinsland, C., Gunson, M., and Beer, R.: Tropospheric emission spectrometer: retrieval method and error analysis, IEEE Transactions on Geoscienc and Remote Sensing, 44, 1297-1307, 2006.

Caulton, D. R., Shepson, P. B., Santoro, R. L., Sparks, J. P., Howarth, R. W., Ingraffea, A. R., Cambaliza, M. O., Sweeney, C., Karion, A., and Davis, K. J.: Toward a better understanding and quantification of methane emissions from shale gas development, Proceedings of the National Academy of Sciences, 111, 6237-6242, 2014.

Etheridge, D. M., Steele, L. P., Francey, R. J., and Langenfelds, R. L.: Atmospheric methane between 1000 AD and present: Evidence of anthropogenic emissions and climatic variability, Journal of Geophysical Research-Atmospheres, 103, 15979-15993, 10.1029/98jd00923, 1998.

Frankenberg, C., Aben, I., Bergamaschi, P., Dlugokencky, E., Van Hees, R., Houweling, S., Van Der Meer, P., Snel, R., and Tol, P.: Global column-averaged methane mixing

ratios from 2003 to 2009 as derived from SCIAMACHY: Trends and variability, Journal of Geophysical Research: Atmospheres (1984–2012), 116, 2011.

Funk, C. C., Theiler, J., Roberts, D. A., and Borel, C. C.: Clustering to improve matched filter detection of weak gas plumes in hyperspectral thermal imagery, IEEE T. Geosci. Remote, 39, 1410-1420, 2001.

Gillespie, A., Rokugawa, S., Matsunaga, T., Cothern, J. S., Hook, S., and Kahle, A. B.: A temperature and emissivity separation algorithm for Advanced Spaceborne Thermal Emission and Reflection Radiometer (ASTER) images, Ieee Transactions on Geoscience and Remote Sensing, 36, 1113-1126, 10.1109/36.700995, 1998.

Hook, S. J., Johnson W. R., and Abrams, M. J.: NASA's Hyperspectral Thermal Emission Spectrometer (HyTES), In Thermal Infrared Remote Sensing, Springer, p.527, 2013.

Hook, S. J., Hulley, G. E., Johnson, W. R., Eng, B., Mihaly, J., Chazanoff S., Vance N., Staniszewski Z., Rivera G., Holmes K. T., and Guillevic P.: The Hyperspectral Thermal Emission Spectrometer (HyTES) – A New Hyperspectral Thermal Infrared Airborne Imager for Earth Science, to be submitted to Remote Sensing of Environment.

Hsu, Y. K., VanCuren, T., Park, S., Jakober, C., Herner, J., FitzGibbon, M., Blake, D. R., and Parrish, D. D.: Methane emissions inventory verification in southern California, Atmospheric Environment, 44, 1-7, 10.1016/j.atmosenv.2009.10.002, 2010.

Hulley, G., *et al.*, High spatial resolution imaging of methane and other trace gas sources with the airborne Hyperspectral Thermal Emission Spectrometer (HyTES), in preparation.

Jeong, S., Hsu, Y. K., Andrews, A. E., Bianco, L., Vaca, P., Wilczak, J. M., and Fischer, M. L.: A multitower measurement network estimate of California's methane emissions,

Journal of Geophysical Research-Atmospheres, 118, 11339-11351, 10.1002/jgrd.50854, 2013.

Kalnay, E., Kanamitsu, M., Kistler, R., Collins, W., Deaven, D., Gandin, L., Iredell, M., Saha, S., White, G., Woollen, J., Zhu, Y., Chelliah, M., Ebisuzaki, W., Higgins, W., Janowiak, J., Mo, K. C., Ropelewski, C., Wang, J., Leetmaa, A., Reynolds, R., Jenne, R., and Joseph, D.: The NCEP/NCAR 40-year reanalysis project, Bulletin of the American Meteorological Society, 77, 437-471, 10.1175/1520-0477(1996)077<0437:tnyrp> 2.0.co;2, 1996.

Kirschke, S., Bousquet, P., Ciais, P., Saunois, M., Canadell, J. G., Dlugokencky, E. J., Bergamaschi, P., Bergmann, D., Blake, D. R., and Bruhwiler, L.: Three decades of global methane sources and sinks, Nature Geoscience, 6, 813-823, 2013.

Kort, E. A., Frankenberg, C., Costigan, K. R., Lindenmaier, R., Dubey, M. K., and Wunch, D.: Four corners: The largest US methane anomaly viewed from space, Geophysical Research Letters, 41, 6898-6903, 2014.

Kuai, L., Worden, J., Kulawik, S. S., Montzka, S. A., and Liu, J.: Characterization of Aura TES carbonyl sulfide retrievals over ocean, Atmospheric Measurement Techniques, 7, 163-172, 10.5194/amt-7-163-2014, 2014.

Lelieveld, J., Crutzen, P. J., and Dentener, F. J.: Changing concentration, lifetime and climate forcing of atmospheric methane, Tellus Series B-Chemical and Physical Meteorology, 50, 128-150, 10.1034/j.1600-0889.1998.t01-1-00002.x, 1998.

McKain, K., Down, A., Raciti, S. M., Budney, J., Hutyra, L. R., Floerchinger, C., Herndon, S. C., Nehrkorn, T., Zahniser, M. S., and Jackson, R. B.: Methane emissions from natural gas infrastructure and use in the urban region of Boston, Massachusetts, Proceedings of the National Academy of Sciences, 201416261, 2015.

Miller, C. E., and Dinardo, S. J.: CARVE: The Carbon in Arctic Reservoirs Vulnerability Experiment, IEEE Aerospace Conf. DOI:10.1109/AERO.2012.6187026, 2012

NOAA: GMD Measurement Locations, National Oceanic & Atmospheric Adminstration (NOAA), Earth System Research Laboratory, Global Measurement Division, 2013.

Peischl, J., Ryerson, T. B., Brioude, J., Aikin, K. C., Andrews, A. E., Atlas, E., Blake, D., Daube, B. C., de Gouw, J. A., Dlugokencky, E., Frost, G. J., Gentner, D. R., Gilman, J. B., Goldstein, A. H., Harley, R. A., Holloway, J. S., Kofler, J., Kuster, W. C., Lang, P. M., Novelli, P. C., Santoni, G. W., Trainer, M., Wofsy, S. C., and Parrish, D. D.: Quantifying sources of methane using light alkanes in the Los Angeles basin, California, Journal of Geophysical Research-Atmospheres, 118, 4974-4990, 10.1002/jgrd.50413, 2013.

Ramaswamy: The Third Assessment Report of the Intergovernmental Panel on Climate Change (eds Hougton, J. T. et al.), Cambridge Univ. Press, 349-416, 2001.

Rodgers, C. D.: Inverse Methods for Atmospheric Sounding: Theory and Practice, World Scientific, London, 256 pp., 2000.

Solomon, S., D. Qin, M. Manning, Z. Chen, M. Marquis, K.B. Averyt,, and (eds.), M. T. a. H. L. M.: IPCC: Climate Change 2007: The Physical Science Basis. Contribution of Working Group I to the Fourth Assessment Report of the Intergrovernmental Panel on Climate Change, Intergovernmental Panel on Climate Change (IPCC), Cambridge Univ. Press, United Kingdom and New York, USA, 996, 2007.

Wennberg, P. O., Mui, W., Wunch, D., Kort, E. A., Blake, D. R., Atlas, E. L., Santoni, G. W., Wofsy, S. C., Diskin, G. S., Jeong, S., and Fischer, M. L.: On the Sources of Methane to the Los Angeles Atmosphere, Environmental Science & Technology, 46, 9282-9289, 10.1021/es301138y, 2012.

Wong, K. W., Fu, D., Pongetti, T. J., Newman, S., Kort, E. A., Duren, R., Hsu, Y. K., Miller, C. E., Yung, Y. L., and Sander, S. P.: Mapping CH_4: $CO2$ ratios in Los Angeles with

CLARS-FTS from Mount Wilson, California, Atmospheric Chemistry and Physics, 15, 241-252, 10.5194/acp-15-241-2015, 2015.

Worden, J., Kulawik, S. S., Shephard, M., Clough, S. A., Worden, H., Bowman, K., and Goldman, A.: Predicted errors of tropospheric emission spectrometer nadir retrievals from spectral window selection, Journal of Geophysical Research, 109, 10.1029/2004jd004522, 2004.

Worden, J., Bowman, K., Noone, D., Beer, R., Clough, S., Eldering, A., Fisher, B., Goldman, A., Gunson, M., Herman, R., Kulawik, S. S., Lampel, M., Luo, M., Osterman, G., Rinsland, C., Rodgers, C., Sander, S., Shephard, M., and Worden, H.: Tropospheric Emission Spectrometer observations of the tropospheric HDO/H2O ratio: Estimation approach and characterization, Journal of Geophysical Research, 111, 10.1029/2005jd006606, 2006.

Worden, J., Kulawik, S., Frankenberg, C., Payne, V., Bowman, K., Cady-Peirara, K., Wecht, K., Lee, J. E., and Noone, D.: Profiles of CH_4, HDO, H_2O, and N_2O with improved lower tropospheric vertical resolution from Aura TES radiances, Atmospheric Measurement Techniques, 5, 397-411, 10.5194/amt-5-397-2012, 2012.

Wunch, D., Wennberg, P. O., Toon, G. C., Keppel-Aleks, G., and Yavin, Y. G.: Emissions of greenhouse gases from a North American megacity, Geophysical Research Letters, 36, 10.1029/2009gl039825, 2009

Young, S. J., Johnson, B. R., and Hackwell, J. A.: An in-scene method for atmospheric compensation of thermal hyperspectral data, Journal of Geophysical Research-Atmospheres, 107, 10.1029/2001jd001266, 2002.

Table 1. CH_4 vertical average below HyTES flight height. In situ CH_4 profile with AK is the in situ data convolved with HyTES averaging kernel.

Unit (ppm)	Background	In plume
In situ CH_4	2.13	3.34
In situ CH_4 with AK	2.02	2.84
HyTES	1.80±0.2	2.86±0.62
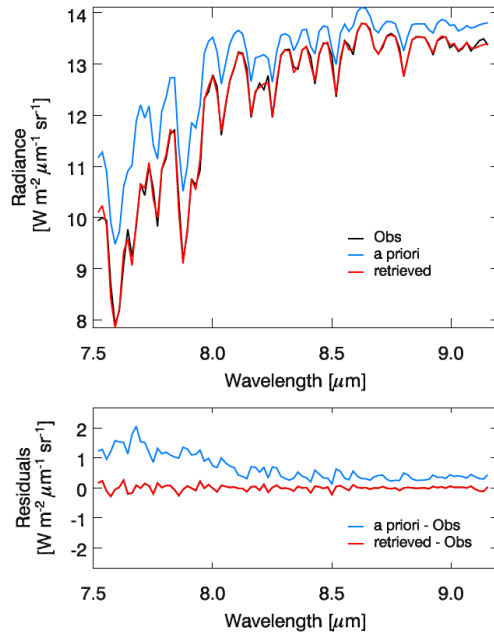
Figure 1. The spectral window for CH$_4$ retrievals. Top: HyTES measured radiances (black) and two model calcuated radiances from *a priori* (blue) and retrieved states (red). Bottom: residuals to the observations.
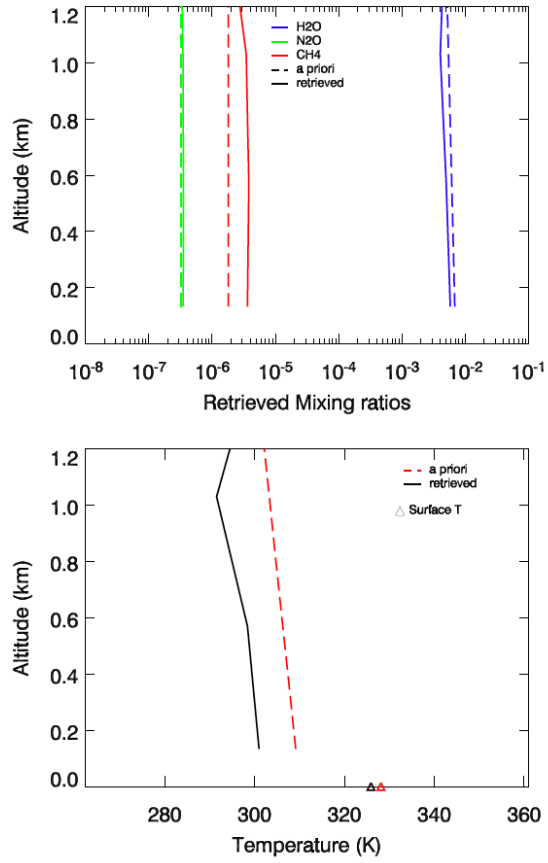
Figure 2. *A priori* (dash or red) and retrieved (solid or black) atmospheric states (H₂O, N₂O, CH₄, temperature, and surface temperature).
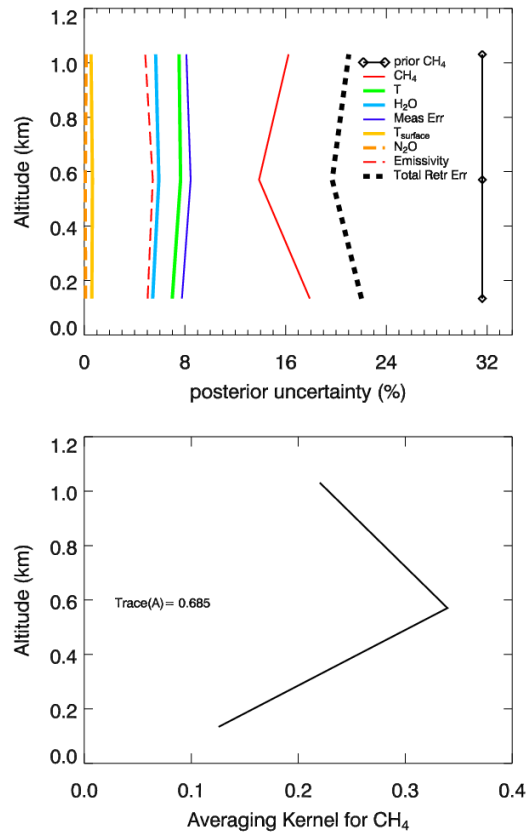
Figure 3. Error budget of the total error in retrieved CH_4. The uncertainties of the *a priori* CH_4 (about 32%) drop to 20%, total error after a retrieval.
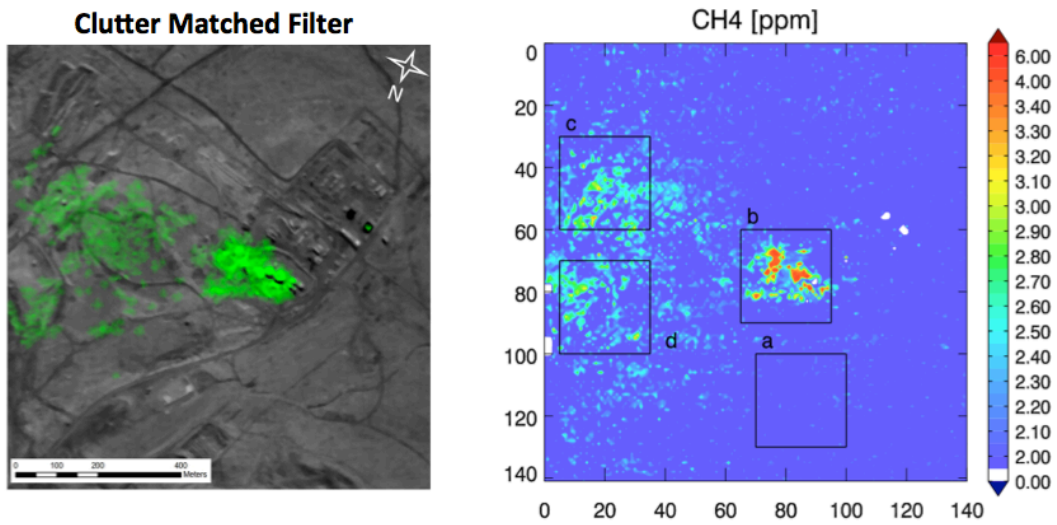
Figure 4. Left: HyTES detected methane plumes (in green) from oil tanks on Feb. 5, 2015 in Kern County, CA and overlayed on grayscale surface temperature image. Right: The methane concentration of the same image from the retrieval estimation. White pixels are missing data.
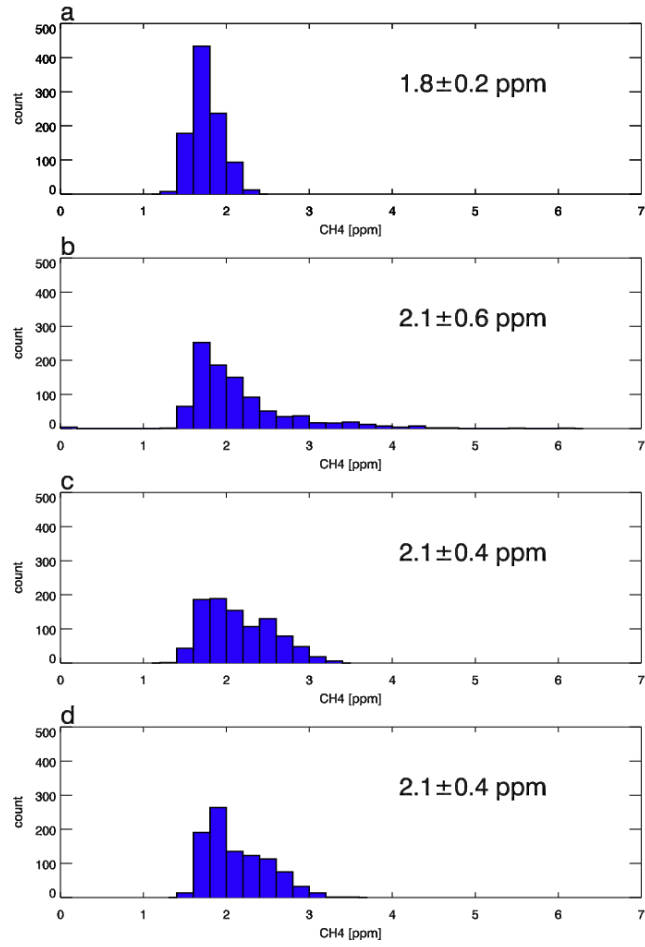
Figure 5. The distributions the methane concentrations in the area of four boxes defined in Figure 4.
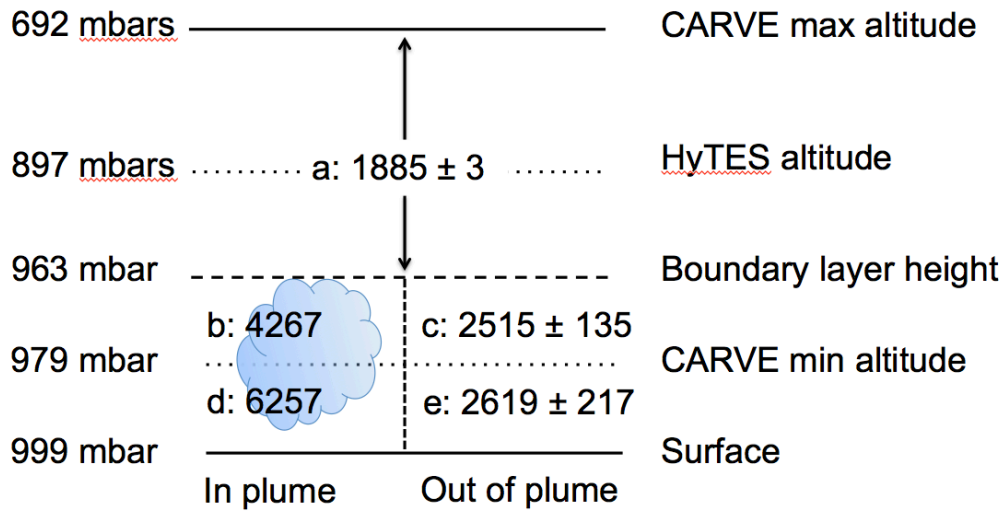
Figure 6. Partial column average to profile CH_4 in the plume and background region with CARVE and vehicle data.